ORIGINAL RESEARCH

# Gadolinium Enhanced T2 FLAIR is an Imaging Biomarker of Radiation Necrosis and Tumor Progression in Patients with Brain Metastases

Chris Heyn, Jonathan Bishop, Alan R. Moody, Tony Kang, Erin Wong, Peter Howard, Pejman Maralani, Sean Symons, Bradley J. MacIntosh, Julia Keith, Mary Jane Lim-Fat, James Perry, Sten Myrehaug, Jay Detsky, Chia-Lin Tseng, Hanbo Chen, Arjun Sahgal, and Hany Soliman

## ABSTRACT

**BACKGROUND AND PURPOSE:** Differentiating radiation necrosis (RN) from tumor progression (TP) after radiotherapy for brain metastases is an important clinical problem requiring advanced imaging techniques which may not be widely available and are challenging to perform at multiple time points. The ability to leverage conventional MRI for this problem, could have meaningful clinical impact. The purpose of this study was to explore contrast enhanced T2 FLAIR (T2FLAIRc) as a new imaging biomarker of RN and TP.

**MATERIALS AND METHODS:** This single-institution retrospective study included patients with treated brain metastases undergoing DSC-MRI between January 2021 and June 2023. Reference standard assessment was based on histopathology or serial follow-up including results of DSC-MRI for a minimum of 6 months from the first DSC-MRI. The index test was implemented as part of the institutional brain tumor MRI protocol and preceded the first DSC-MRI. T2FLAIRc and gadolinium enhanced T1 MPRAGE (T1c) signal were normalized against normal brain parenchyma and expressed as z-score. Mean signal intensity of enhancing disease for RN and TP groups were compared using unpaired t-test. Receiver operator characteristic (ROC) curves and area under the ROC curve (AUC) were derived by bootstrapping. DeLong test was used to compare AUC.

**RESULTS:** 56 participants (mean age, 62 years +/- 12.7 [SD]; 39 females); 28 RN, 28 TP were evaluated. The index MRI was performed on average 73 days +/- 34 [SD] before the first DSC-MRI. Significantly higher z-scores were found for RN using T2FLAIRc (8.3 versus 5.8, $p<0.001$) and T1c (4.1 versus 3.5, $p=0.02$). AUC for T2FLAIRc (0.83, 95% CI, 0.72-0.92) was greater than T1c (0.70, 95% CI, 0.56-0.83) ($p = 0.04$). The AUC of DSC derived rCBV (0.82, 95% CI, 0.70-0.93) was not significantly different from T2FLAIRc ($p = 0.9$).

**CONCLUSIONS:** A higher normalized T1c and T2FLAIRc signal intensity was found for RN. In a univariable test, mean T2FLAIRc signal intensity of enhancing voxels showed good discrimination performance for distinguishing RN from TP. The results of this work demonstrate the potential of T2FLAIRc as an imaging biomarker in the work-up of RN in patients with brain metastases.

**ABBREVIATIONS:** AUC = area under the receiver operating characteristic curve; RN = radiation necrosis; ROC = receiver operating characteristic; SRS = stereotactic radiosurgery; T1c = contrast enhanced T1; T2FLAIRc = contrast enhanced T2 FLAIR; TP = tumor progression.

Received month day, year; accepted after revision month day, year.
From the Department of Medical Imaging, Sunnybrook Health Sciences Centre, Toronto, Ontario, Canada (C.H., J.B., A.R.M., T.K., E.W., P.H., P.M., S.S.), Department of Medical Imaging, University of Toronto, Toronto, Ontario, Canada (C.H., A.R.M., T.K., E.W., P.H., P.M., S.S.), Sunnybrook Research Institute, Sunnybrook Health Sciences Centre, Toronto, Ontario, Canada (C.H., A.R.M., P.M., S.S., B.J.M.), Department of Anatomy and Pathology, Sunnybrook Health Sciences Centre, Toronto, Ontario, Canada (J.K.), Division of Neurology, Department of Medicine, Sunnybrook Health Sciences Centre, Toronto, Ontario, Canada (M.J.L, J.P.), Department of Radiation Oncology, Sunnybrook Health Sciences Centre, Toronto, Ontario, Canada (S.M.,J.D., C.T., H.C., A.S., H.S.)

Chris Heyn, Jonathan Bishop, Hany Soliman, and Alan R. Moody are coinventors on a provisional patent assigned to Sunnybrook Research Institute (US Provisional Patent No. 63/537,092) for the methodology described in this article.

Please address correspondence to Chris Heyn, MD PhD, Department of Medical Imaging, Sunnybrook Health Sciences Centre, 2075 Bayview Ave., Toronto, Ontario, Canada M4N 3M5; chris.heyn@utoronto.ca.

## SUMMARY SECTION

**PREVIOUS LITERATURE:** Differentiating radiation necrosis from tumor progression using conventional MRI is challenging. Previous studies using commonly acquired pulse sequences such as T2, T2 FLAIR and contrast enhanced T1 in qualitative and quantitative approaches have shown limited diagnostic performance or may be challenging to implement.

**KEY FINDINGS:** In the present study, we identify contrast enhanced T2 FLAIR as an imaging biomarker of radiation necrosis and tumor progression in patients with brain metastases. Normalized contrast enhanced T2 FLAIR signal intensity was shown to be significantly higher in cases of radiation necrosis compared to tumor progression. Utilizing contrast enhanced T2 FLAIR signal intensity, radiation necrosis and tumor progression could be differentiated with a diagnostic performance comparable to DSC perfusion.

**KNOWLEDGE ADVANCEMENT:** Contrast enhanced T2 FLAIR has diagnostic potential for differentiating radiation necrosis from tumor progression in patients with brain metastases. Further work is needed to determine the optimal m**ethodology for using** this imaging

## INTRODUCTION

Brain metastases are the most common adult malignant intracranial tumors presenting in 20-40% of patients with solid malignancies in the course of their disease (1). Stereotactic radiosurgery (SRS) is a key treatment indicated in patients with a limited number of brain metastases (2-6). Despite excellent rates of local control, there is a spectrum of MR imaging changes that can occur weeks to several years after treatment and can mimic tumor progression (TP) both clinically and radiologically. The term radiation-induced contrast enhancement has been coined to describe non-tumor enhancement which results from radiation treatment (7). It encompasses pseudoprogression, a transient increase in the size of enhancement (usually within the first three months), and radiation necrosis (RN), a serious and late complication of SRS.

The incidence of RN after SRS varies in the literature, with estimates of up to 30% (8, 9). Symptomatic RN is seen in about half of these cases, which results in significant morbidity and death in some cases (10-12). Early intervention with corticosteroids, bevacizumab, surgery or laser interstitial thermal therapy can improve outcomes in symptomatic RN (13, 14) making timely diagnosis critical for patient management.

Distinguishing RN from TP continues to be a problem in neuro-oncology. Histopathology is the gold standard for diagnosis but may not be feasible in all cases and often shows a mixture of RN and viable tumor. Advanced imaging techniques, including DSC perfusion, MR spectroscopy, chemical exchange saturation transfer, and PET (9) have been increasingly adopted but may be difficult to acquire longitudinally and may not be available to all centers. Approaches which can distinguish RN from TP on conventional MRI sequences could have significant advantages. First, the diagnostic work-up starts with an analysis of conventional MRI with the subsequent addition of advanced imaging techniques if they are available (15). Second, many patients undergo multiple serial follow-up studies which is more easily accomplished with conventional MRI.

Differentiating RN and TP on conventional MRI has proven to be challenging. Semi-quantitative and qualitative approaches such as measurement of the Lesion Quotient or T1-T2 mismatch (16, 17), have been proposed, but these have failed to be reproduced with sufficient sensitivity and specificity to be clinically useful (18). More recently, contrast clearance analysis (19) which involves measuring changes in contrast enhancement on T1-weighted sequences performed at early (5 minute) and delayed (>60 minute) time points using image subtraction has been investigated, but the practicality of a delayed contrast-enhanced MRI is challenging and may not be feasible in all radiology departments. Radiomics and deep learning models applied to conventional MRI hold promise with diagnostic performance approaching that of DSC-perfusion (20, 21).

Consensus guidelines for brain tumor imaging protocols currently recommend pre-contrast T2 FLAIR (22), however, there is growing evidence that contrast enhanced T2 FLAIR may offer additional diagnostic information. At our institution, contrast enhanced T2 FLAIR is routinely performed instead of pre-contrast T2 FLAIR for several reasons including reducing protocol time by utilizing the time between contrast administration and acquisition of post contrast T1 MPRAGE and improving the detection of leptomeningeal disease (23-26). In the present work, we evaluate contrast enhanced T2 FLAIR as a potential new imaging biomarker for distinguishing RN from TP. We hypothesize that patients with RN and TP will demonstrate significant differences in normalized contrast enhanced T2 FLAIR signal intensity which can be used to distinguish RN from TP.

## MATERIALS AND METHODS

### *Patients*

Adult (>18 years-old) patients with brain metastases previously treated with SRS or fractionated stereotactic radiotherapy, with increasing size of enhancement detected on institutional MRI (index MRI) and who underwent subsequent work-up with a DSC-MRI to differentiate RN from TP were identified for this retrospective single-center study. Institutional research ethics board approved the study (REB #5431) with waiver of informed consent. The radiology search engine Montage (Montage Healthcare Solutions, Philadelphia, Pa) was used to identify consecutive studies that contained the word "perfusion" for brain MRI reports between January 1, 2021 and June 30, 2023. For patients with multiple perfusion studies, the earliest perfusion study was used. Inclusion criteria were: (*a*) Prior SRS or fractionated stereotactic radiotherapy for brain metastases, (*b*) increase in enhancement detected on index MRI performed within 6 months of the first DSC study, and (*c*) tumor size ≥ 10 mm measured on contrast-enhanced series from the index MRI. Exclusion criteria: (*a*) hemorrhagic metastasis (blooming on GRE in >50% of lesion) or containing intrinsic T1 hyperintensity, (*b*) extra-axial metastasis, (*c*) insufficient follow-up or uncertainty in diagnosis after clinical review, (*d*) radiation or surgery between index MRI and DSC study, (*e*) corruption of index MRI by artifact. Previous surgery with surgical cavity radiation and prior whole brain radiation were not exclusionary. The study conformed with the Standards for Reporting of Diagnostic Accuracy Studies (STARD) 2015 (27).

### *MRI Acquisition*

Imaging was performed on 1.5T (MAGNETOM Aera or Sola, Siemens) or 3T (MAGNETOM Vida, Siemens) MRI systems using body transmit and 20-channel head and neck receiver coils. The institutional brain tumor imaging protocol included axial RESOLVE DWI (b-values = 0 and 1000 s/mm$^2$ , TR = 3650 to 7390 ms, TE = 67.2 to 72.2 ms, in-plane resolution 0.54 x 0.54 mm$^2$ to 1.25 x 1.25 mm$^2$, slice thickness 5 mm), T2 FLAIR acquired in the axial plane (TR = 9000 ms, TE = 80 to 108 ms, TI = 2500 ms, in-plane resolution 0.75 x 0.75

$mm^2$ to 0.83 x 0.83 $mm^2$, slice thickness 3 or 5 mm) immediately after intravenous injection of a bolus of gadolinium contrast agent (Gadobutrol, Bayer) at a dose of 0.1 mmol/kg followed by a 20 mL saline flush, and 3D T1 MPRAGE (TR = 1800 or 2240 ms, TE = 2.5 or 3 ms, flip angle = 8°, resolution 1 x 1 x 1 $mm^3$) acquired after T2 FLAIR. For the purposes of the current study, post-gadolinium T2 FLAIR and T1 MPRAGE are referred to as T2FLAIRc and T1c respectively.

For the DSC-MRI exam, all patients received a total gadolinium dose of 0.1 mmol/kg split into two with half dose administered as a preload bolus for leakage correction and the second half administered during the DSC acquisition. DSC-MRI was acquired in the axial plane using single-shot gradient echo EPI sequence (TR = 1830 or 2080 ms, TE = 30 or 31 ms, flip angle = 90°, resolution 1 x 1 x 3 $mm^3$, 26 slices, 120 phases) during the first pass of a bolus of gadolinium at a rate of 5 mL/s on phase 30 of the perfusion sequence followed by a 20 mL saline flush injected at the same rate.

### *Image Processing and Analysis*

Tumors were segmented using a Matlab (Mathworks) implementation of the Background LAyer STatistics (BLAST) methodology which has been previously described (28). Segmentations of enhancing tumor were performed without knowledge of the lesion outcome or results of DSC perfusion by a neuroradiologist (CH) with 11 years of post-graduate work experience. T2FLAIRc and T1c signal intensities from the entire tumor volume were normalized to background normal brain parenchyma and expressed as z-score. Mean time for 3D tumor segmentation and signal intensity measurement was 1.2 minutes/tumor. Details of the algorithm are included in Online Supplemental Data.

Perfusion maps were generated in syngo.via (Siemens) using a localized AIF algorithm and leakage correction. A Matlab script was written to derive rCBV maps and to overlay an ROI defined by a segmentation mask of enhancing tumor. The rCBV maps were generated by normalizing CBV maps to contralateral normal appearing white matter using a circular ROI placed at or close to the same slice as the enhancing brain tumor.

### *Reference Standard Assessment of Lesion Outcome*

Reference standard assessment of RN and TP was determined by a neuropathologist (JK) with 16 years of experience and a radiation oncologist (HS) with 13 years of experience, both blinded to the results of the index test. If histopathology was available, the lesion was considered TP if the histological assessment by the neuropathologist consisted of >20% tumor (29). If histopathology was not available, then the clinical outcome from serial imaging follow-up MR examinations were based on the Response Assessment in Neuro-Oncology Brain Metastases criteria (30) incorporating the results of DSC perfusion from radiology reports with a minimum of 6 months follow-up from the time of the first perfusion study.

### *Statistical Analysis*

Statistical analysis was performed using Matlab. Shapiro-Wilk test was used to test for normality. Categorical variables are presented as a proportion or percentage of patients. Continuous variables are presented as a mean ± SD for normally distributed variables, and median with IQR for non-normally distributed variables. For patient demographics, categorical variables were compared using the $\chi^2$ or Fisher exact test, where appropriate. Continuous variables were compared using the Wilcoxon rank-sum test for non-parametric group comparison and *t*-test for parametric group comparisons. Results were considered significant if the *p* value was less than 0.05.

Receiver operating characteristic (ROC) curves, mean area under the ROC curve (AUC) and 95% CI were derived by bootstrapping using 1000 iterations. Additionally, ROC curves, AUC and 95% CI for logistic regression models predicting disease status from T2FLAIRc, T1c, rCBV and combinations of these parameters were performed using leave one out cross-validation. Optimal cut-point, sensitivity and specificity were determined by Youden's index, and the DeLong test was used to compare AUC. A logistic regression model was used to assess the association between disease status predicted by T2FLAIRc signal intensity and field strength.

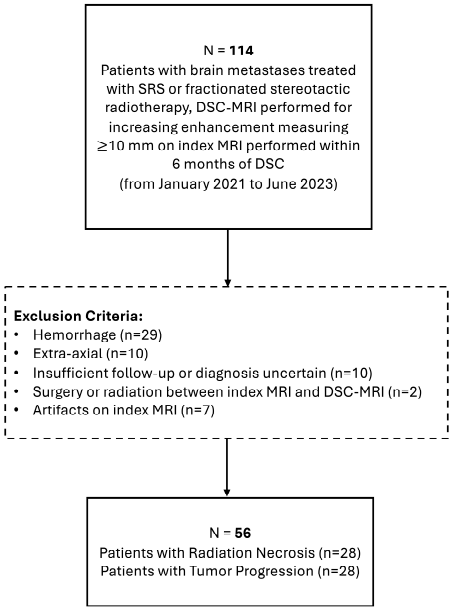


**FIG 1**. Flow diagram for patient selection and exclusion.

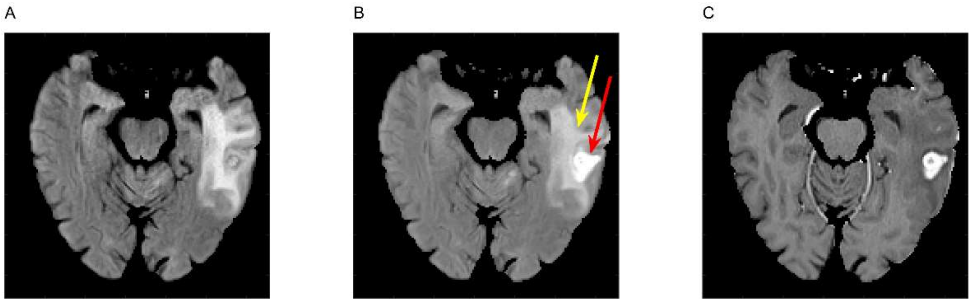


**FIG 2**. Unenhanced T2 FLAIR **(A)**, enhanced T2 FLAIR (T2FLAIRc) **(B)** and enhanced T1 MPRAGE (T1c) **(C)** are shown for a treated brain metastasis in the left temporal lobe (radiation necrosis case). T2FLAIRc demonstrates hybrid contrast between T2 FLAIR and T1c and show edema (yellow arrow) and contrast enhancement (red arrow).

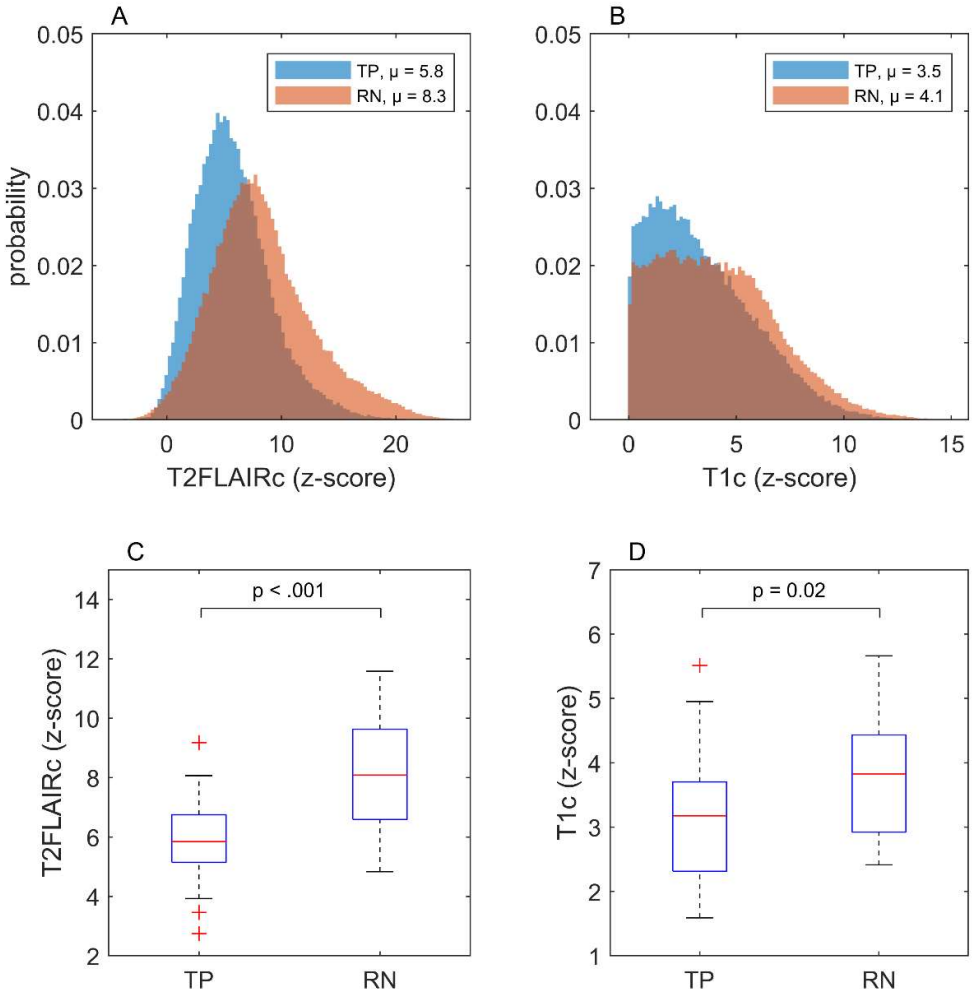


**FIG 3.** Histograms and box-plots illustrating the complete set of all enhancing voxels across all tumor progression (TP) and radiation necrosis (RN) patients for contrast enhanced T2 FLAIR (T2FLAIRc) and T1 (T1c). Mean signal intensities for each group are indicated in the figure legends for the histograms. The box plots depict the mean and interquartile range. *p* values for unpaired *t*-test are shown and considered significant for $p<0.05$.

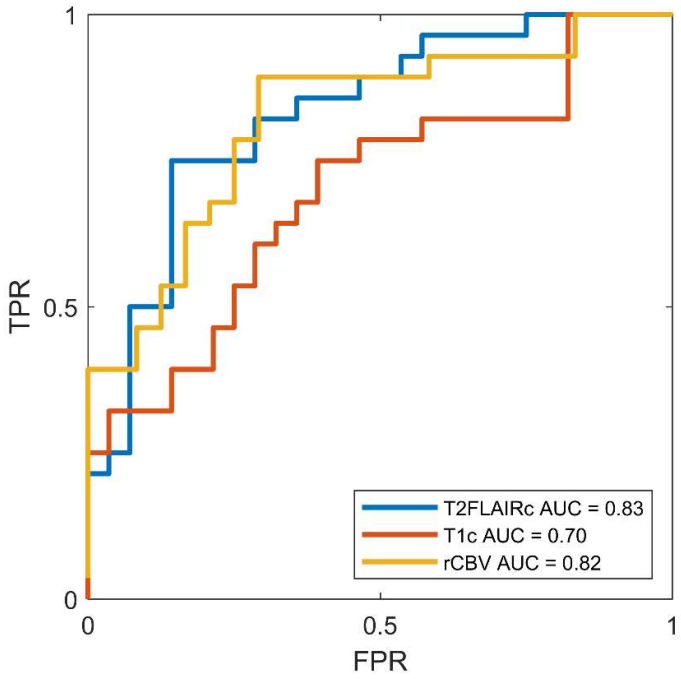


**FIG 4**. Receiver operating characteristic (ROC) curves for contrast enhanced T2 FLAIR (T2FLAIRc), T1 (T1c) and rCBV from DSC perfusion. AUC for T2FLAIRc was significantly higher compared to T1c ($p$ = 0.04) but not for rCBV ($p$ = 0.9). AUC, area under the ROC curve; FPR, false positive rate; TPR, true positive rate.

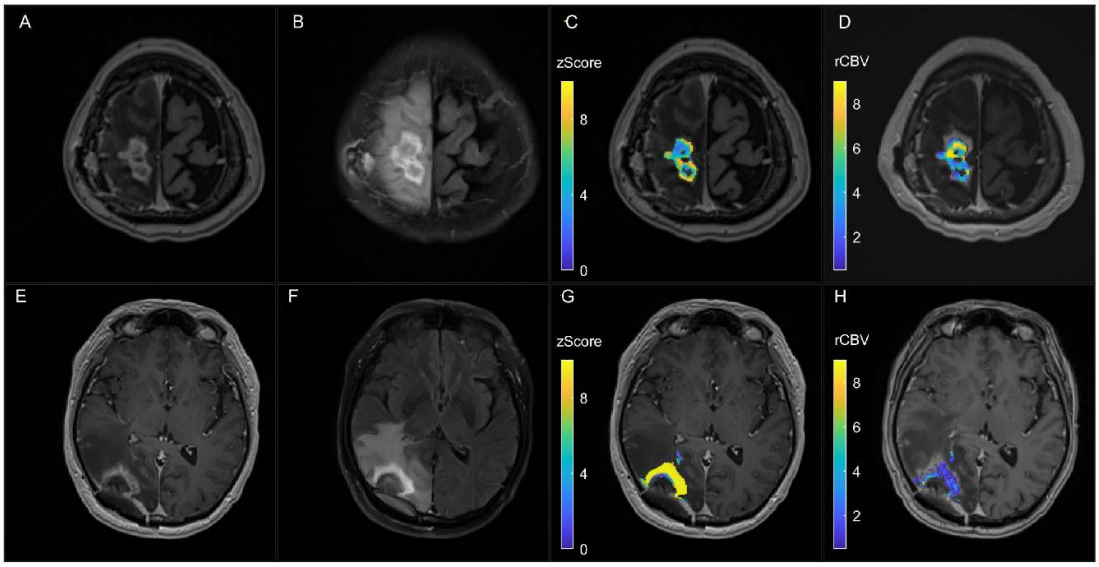


**FIG 5**. Comparison of contrast enhanced T2 FLAIR (T2FLAIRc) z-score parameter map with rCBV map for cases of tumor progression (TP, top row) and radiation necrosis (RN, bottom row). **(A, E)** Axial contrast enhanced T1 MPRAGE (T1c) and **(B, F)** corresponding T2FLAIRc. **(C, G)** T2FLAIRc z-score for enhancing tumor voxels overlayed on T1c images show lower values (mean, 5.8 ± 2.0 [SD]) for TP and higher values (mean, 12.6 ± 5.7 [SD]) for RN. **(D, H)** rCBV map from follow-up dynamic susceptibility perfusion MRI show higher values for TP (mean, 4.8 ± 2.3 [SD]) and lower values for RN (mean, 1.3 ± 1.2 [SD]).

## RESULTS

### *Patient Characteristics*

Of the 114 patients initially identified, 29 were excluded because the tumor was hemorrhagic; ten were excluded because the tumor was extra-axial; ten were excluded because there was insufficient follow-up or the diagnosis was uncertain; seven were excluded because of artifacts; and two were excluded because of treatment occurring between the index MRI and DSC study (Figure 1). A total of 56 patients were thus included and determined to be RN (n = 28) and TP (n = 28). Median time between radiation and DSC study was 296 days (IQR, 222-588)) and 394 days (IQR, 347-586) for the RN and TP groups respectively ($p$=0.06). Mean time between index MRI and DSC study was 78 days ± 35 [SD] and 68 days ± 32 [SD] for the RN and TP groups respectively ($p$=0.30). Diagnosis of RN or TP was made by histopathology in 14 (25%) cases and clinical follow-up in 42 (75%) cases. The median time between the DSC study and histopathology was 75 days (IQR, 52-165). For histopathology-proven cases, assessment by RANO and histology were concordant in 10/14 (71%) of cases. For the index MRI, 12 patients were scanned at 1.5T and 16 were scanned at 3T in the RN group, and 16 patients were scanned at 1.5T and 12 patients were scanned at 3T in the TP group; ($p$=0.42). DSC was not diagnostic in 4 patients: 1 lesion obscured by artifact from the skull base, 1 lesion was too small to characterize, and 2 lesions were not covered by the DSC acquisition. Table 1 summarizes demographics, tumor characteristics and MRI data.

### *Signal Intensity Distributions for Tumor Progression and Radiation Necrosis*

Images of a treated metastasis (radiation necrosis case) are shown to illustrate the similarities and differences in image contrast for unenhanced T2 FLAIR, T2FLAIRc and T1c (Figure 2). T2FLAIRc demonstrates a hybrid contrast of T2 FLAIR and T1c with areas of edema and gadolinium contrast enhancement appearing hyperintense.

Figure 3 shows histograms and box plots of normalized signal intensity for the TP and RN groups. The data shown are for all enhancing voxels for the 3D tumor volume. Signal intensity for T2FLAIRc showed a significantly higher mean for RN compared to TP (8.3 versus 5.8, $p$<0.001). A significantly higher mean signal intensity for T1c was also found for RN compared to TP (4.1 versus 3.5, $p$=0.02).

### *Diagnostic Performance of T2FLAIRc, T1c and DSC Perfusion*

The AUC derived from bootstrapping was 0.83 (95% CI, 0.72-0.92) and 0.70 (95% CI, 0.56-0.83) for T2FLAIRc and T1c respectively ($p$ = 0.04). The sensitivity, specificity, optimal cut-point were 75%, 86%, 6.2 and 75%, 61%, 3.6 for T2FLAIRc and T1c, respectively. The AUC for DSC perfusion rCBV was 0.82 (95% CI, 0.70-0.93) and not significantly different from T2FLAIRc ($p$ = 0.9). The sensitivity, specificity of rCBV were 89% and 61% respectively. The optimal cut-point for rCBV derived by Youden's index was 2.1. ROC curves are illustrated in Figure 4.

Logistic regression models in leave one out cross-validation showed AUC=0.78 (95% CI, 0.67-0.91), 0.59 (95% CI, 0.53-0.82) and 0.79 (95% CI, 0.70-0.92) for T2FLAIRc, T1c and rCBV respectively. AUC=0.82 (95% CI, 0.76-0.85) for the combined model with all three parameters and was not significantly different compared to T2FLAIRc or rCBV alone ($p$=0.26 and 0.49 respectively). Logistic regression analysis showed that field strength was not a significant predictor of disease status measured by T2FLAIRc ($p$ = 0.56).

### *T2FLAIRc Parameter Maps*

Figure 5 shows T2FLAIRc parameter maps for a case of TP and RN. For the parameter maps, the color-coded z-score of normalized T2FLAIRc signal is shown for enhancing voxels overlayed on the T1c image. Corresponding rCBV maps for the approximate same slice from the follow-up DSC study are shown for comparison.

## DISCUSSION

Differentiating RN from TP on imaging continues to be a problem. The imaging work-up begins with an evaluation of conventional MRI, but given its poor diagnostic performance, multiple longitudinal follow-up studies with the addition of advanced imaging methods such as DSC-MRI and PET are often performed. In the present study we demonstrated that normalized T1c and T2FLAIRc, measured across all enhancing tumor voxels, is significantly higher for RN than TP. Utilizing a univariable test of normalized T2FLAIRc signal intensity requiring approximately 1 minute of user time/tumor, RN and TP can be distinguished with an AUC of 0.83 which was not significantly different than DSC perfusion performed approximately 2 months later.

The findings of a higher T1c and T2FLAIRc signal intensity in RN compared to TP are consistent with prior radiomics studies. One of the largest was a study of 66 patients (77 lesions) which examined 51 radiomics features in images from a conventional MRI protocol that included unenhanced T2 FLAIR and contrast enhanced T1 weighted sequences (31). The top radiomics feature in that study was minimum T1c which is a first order radiomics feature corresponding to the minimum gray level intensity of contrast enhanced T1 and showed a higher mean value for RN compared to TP with an AUC of 0.70 in univariable analysis. Minimum T2 FLAIR, corresponding to the minimum gray level signal intensity of unenhanced T2 FLAIR ranked 8$^{th}$ with an AUC of 0.65 in univariable analysis.

The physical basis for differences in T2FLAIRc and T1c signal intensity between TP and RN has not been elucidated in this study but is likely multifactorial. One potential explanation is how contrast leakage affects T1 and T2* relaxivity in tumor and RN (32, 33). T1 shortening effects of extravasated gadolinium will increase signal intensity on both T1c and T2FLAIRc. This effect will be greater for disease with higher vascular permeability and larger extravascular extracellular water pools. Countering this are T2* effects which will tend to reduce signal intensity. Extravasated gadolinium will undergo compartmentalization within the extravascular extracellular space resulting in bulk magnetic susceptibility effects and shortening of T2*. Differences in extracellular tissue microstructure could lead to differential compartmentalization of gadolinium and may also contribute to the signal intensity differences observed in this study. Because RN is expected to have a lower cellularity and less structured extravascular-extracellular compartment, there will be less T2* shortening from compartmentalized gadolinium resulting in higher signal intensity compared to tumor. Ultimately, numerical simulations and experiments examining these effects could provide useful insights and guide pulse sequence design to exploit this contrast mechanism.

An attractive feature of T2FLAIRc signal intensity is the ability to qualitatively inspect images or produce parametric maps (Figure 5) at a spatial resolution equivalent to conventional MRI. While a rigorous analysis of these images or maps was not undertaken, spatial heterogeneity in T2FLAIRc was observed with similarities to the heterogeneity observed with rCBV maps. Qualitative radiographic interpretation of these maps by a human reader may provide additional insights for distinguishing TP from RN which could be used to guide the development of radiomics or deep learning models and verify their predictions. Precisely how images or normalized parametric MR maps are used in conjunction with advanced imaging techniques like DSC and how this approach compares to other existing methods is an open question requiring further study.

There are limitations to a simple univariable test based on a normalized signal intensity. For example, the normalized signal intensity used in this study is a measure of contrast-to-noise ratio and can be affected by imaging parameters such as field strength. The results of a logistic regression showed field strength was not a significant predictor of disease status measured by T2FLAIRc. Other differences in MR hardware, pulse sequence parameters and contrast dose timing between different sites and vendors could also affect normalized signal intensity and were not explicitly assessed in this study. An evaluation of multi-site data utilizing a variety of imaging hardware and protocols and the development of multivariable radiomics or deep learning models to mitigate these effects is a logical next step. Another limitation is the exclusion of lesions with extensive blooming on GRE which were omitted because of the potential of hemosiderin to alter tumor relaxivity and reduce the observed signal intensity of enhancing tumor on T2FLAIRc and T1c. Lesions with intrinsic T1 hyperintensity resulting from methemoglobin or other causes were also excluded as the methodology employed to determine contrast enhancement (normalized T1c signal intensity greater than background brain) would not be able to distinguish intrinsic T1 hyperintensity from contrast enhancement. Other limitations of the present study include the inherent biases and limited data of a retrospective study design which relied heavily on clinical follow-up and precluded a comparison of T2FLAIRc with unenhanced T2 FLAIR which is not routinely acquired at our institution. The current study is also limited by a small sample size and not designed or powered to evaluate the diagnostic superiority/inferiority of normalized T2FLAIRc against DSC perfusion.

**Table 1**: Patient and Tumor Characteristics.

| Characteristic | Total (*n*=56) | Tumor Progression (*n*=28) | Radiation Necrosis (*n*=28) | *p* Value |
|---|---|---|---|---|
| Age (yr) | 61.9±12.7 | 60.2±12.5 | 63.6±12.8 | 0.32 |
| Sex | | | | 1.00 |
| Male | 17 (30.4%) | 8 (28.5%) | 9 (32%) | |
| Female | 39 (69.6%) | 20 (71.4%) | 19 (68%) | |
| Primary Cancer Type | | | | 0.50 |
| NSCLC | 25 (44.6%) | 14 (50%) | 11 (39.2%) | |
| Breast | 18 (32.1%) | 9 (32.1%) | 9 (32.1%) | |
| Melanoma | 4 (7.1%) | 1 (3.6%) | 3 (10.7%) | |
| RCC | 4 (7.1%) | 1 (3.6%) | 3 (10.7%) | |
| Other | 5 (8.9%) | 3 (10.7%) | 2 (7.1%) | |
| Total Dose (Gy) | 25 (IQR,20 –30) | 23.3 (IQR,19.5 –27.5) | 27.3 (IQR,20 –30) | 0.25 |
| # Fractions | 3 (IQR,1–5) | 3 (IQR,1–5) | 5 (IQR,1–5) | 0.72 |
| Time from SRS to DSC (d) | 358 (IQR,262-586) | 394 (IQR,347-586) | 296 (IQR,222-588) | 0.06 |
| Time from index MR to DSC (d) | 73±34 | 68±32 | 78±35 | 0.30 |
| Systemic Therapy | 25 (44.6%) | 12 (42.9%) | 13 (46.4%) | 1.00 |
| Lesion Outcome | | | | 0.76 |
| Pathology | 14 (25%) | 8 (29%) | 6 (21%) | |
| Follow-up | 42 (75%) | 20 (71%) | 22 (79%) | |
| Scanner Field Strength | | | | 0.42 |
| 1.5T | 28 (50%) | 16 (57%) | 12 (43%) | |
| 3T | 28 (50%) | 12 (43%) | 16 (57%) | |

Note. -- Categorical variables are presented as a proportion or percentage of patients. Continuous variables are presented as a mean ± SD for normally distributed variables, and median with interquartile range (IQR) for non-normally distributed variables. Categorical variables were compared using the $\chi^2$ or Fisher exact test, where appropriate. Continuous variables were compared using the Wilcoxon rank-sum test for non-parametric group comparison and *t*-test for parametric group comparisons. Results were considered significant if the *P* value was less than 0.05. NSCLC = non-small cell lung cancer, RCC = renal cell carcinoma

## CONCLUSIONS

In summary, we demonstrate significant differences in normalized contrast enhanced T1 and T2 FLAIR signal intensity for treated brain metastases. Contrast enhanced T2 FLAIR signal intensity can distinguish radiation necrosis and tumor progression with an AUC similar to DSC perfusion. The results of this work point to the diagnostic potential of contrast enhanced T2 FLAIR for diagnosing radiation necrosis and present opportunities for the development of new qualitative and quantitative methodologies to exploit this contrast mechanism.

## REFERENCES


1. Tsao MN, Xu W, Wong RK, Lloyd N, Laperriere N, Sahgal A, et al. Whole brain radiotherapy for the treatment of newly diagnosed multiple brain metastases. Cochrane Database Syst Rev. 2018;1(1):CD003869. Epub 20180125. doi: 10.1002/14651858.CD003869.pub4. PubMed PMID: 29365347; PubMed Central PMCID: PMC6491334.

2. Chang EL, Wefel JS, Hess KR, Allen PK, Lang FF, Kornguth DG, et al. Neurocognition in patients with brain metastases treated with radiosurgery or radiosurgery plus whole-brain irradiation: a randomised controlled trial. Lancet Oncol. 2009;10(11):1037-44. Epub 20091002. doi: 10.1016/S1470-2045(09)70263-3. PubMed PMID: 19801201.

3. Aoyama H, Shirato H, Tago M, Nakagawa K, Toyoda T, Hatano K, et al. Stereotactic radiosurgery plus whole-brain radiation therapy vs stereotactic radiosurgery alone for treatment of brain metastases: a randomized controlled trial. JAMA. 2006;295(21):2483-91. doi: 10.1001/jama.295.21.2483. PubMed PMID: 16757720.

4. Brown PD, Jaeckle K, Ballman KV, Farace E, Cerhan JH, Anderson SK, et al. Effect of Radiosurgery Alone vs Radiosurgery With Whole Brain Radiation Therapy on Cognitive Function in Patients With 1 to 3 Brain Metastases: A Randomized Clinical Trial. JAMA. 2016;316(4):401-9. doi: 10.1001/jama.2016.9839. PubMed PMID: 27458945; PubMed Central PMCID: PMC5313044.

5. Kocher M, Soffietti R, Abacioglu U, Villa S, Fauchon F, Baumert BG, et al. Adjuvant whole-brain radiotherapy versus observation after radiosurgery or surgical resection of one to three cerebral metastases: results of the EORTC 22952-26001 study. J Clin Oncol. 2011;29(2):134-41. Epub 20101101. doi: 10.1200/JCO.2010.30.1655. PubMed PMID: 21041710; PubMed Central PMCID: PMC3058272.

6. Yamamoto M, Sato Y, Higuchi Y, Kasuya H, Barfod BE. A Cohort Study of Stereotactic Radiosurgery Results for Patients With 5 to 15 Versus 2 to 4 Brain Metastatic Tumors. Adv Radiat Oncol. 2020;5(3):358-68. Epub 20191126. doi: 10.1016/j.adro.2019.11.001. PubMed PMID: 32529129; PubMed Central PMCID: PMC7276677.

7. Lutgendorf-Caucig C, Pelak M, Hug E, Flechl B, Surbock B, Marosi C, et al. Prospective Analysis of Radiation-Induced Contrast Enhancement and Health-Related Quality of Life After Proton Therapy for Central Nervous System and Skull Base Tumors. Int J Radiat Oncol Biol Phys. 2024;118(5):1206-16. Epub 20240118. doi: 10.1016/j.ijrobp.2024.01.007. PubMed PMID: 38244874.

8. Aizer AA, Lamba N, Ahluwalia MS, Aldape K, Boire A, Brastianos PK, et al. Brain metastases: A Society for Neuro-Oncology (SNO) consensus review on current management and future directions. Neuro Oncol. 2022;24(10):1613-46. doi: 10.1093/neuonc/noac118. PubMed PMID: 35762249; PubMed Central PMCID: PMC9527527.

9. Mayo ZS, Billena C, Suh JH, Lo SS, Chao ST. The dilemma of radiation necrosis from diagnosis to treatment in the management of brain metastases. Neuro Oncol. 2024;26(12 Suppl 2):S56-S65. doi: 10.1093/neuonc/noad188. PubMed PMID: 38437665; PubMed Central PMCID: PMC10911797.

10. Minniti G, Clarke E, Lanzetta G, Osti MF, Trasimeni G, Bozzao A, et al. Stereotactic radiosurgery for brain metastases: analysis of outcome and risk of brain radionecrosis. Radiat Oncol. 2011;6:48. Epub 20110515. doi: 10.1186/1748-717X-6-48. PubMed PMID: 21575163; PubMed Central PMCID: PMC3108308.

11. Faruqi S, Ruschin M, Soliman H, Myrehaug S, Zeng KL, Husain Z, et al. Adverse Radiation Effect After Hypofractionated Stereotactic Radiosurgery in 5 Daily Fractions for Surgical Cavities and Intact Brain Metastases. Int J Radiat Oncol Biol Phys. 2020;106(4):772-9. Epub 20200109. doi: 10.1016/j.ijrobp.2019.12.002. PubMed PMID: 31928848.

12. Soliman H, Myrehaug S, Tseng CL, Ruschin M, Hashmi A, Mainprize T, et al. Image-Guided, Linac-Based, Surgical Cavity-Hypofractionated Stereotactic Radiotherapy in 5 Daily Fractions for Brain Metastases. Neurosurgery. 2019;85(5):E860-E9. doi: 10.1093/neuros/nyz162. PubMed PMID: 31173150.

13. Ahluwalia M, Barnett GH, Deng D, Tatter SB, Laxton AW, Mohammadi AM, et al. Laser ablation after stereotactic radiosurgery: a multicenter prospective study in patients with metastatic brain tumors and radiation necrosis. J Neurosurg. 2018;130(3):804-11. doi: 10.3171/2017.11.JNS171273. PubMed PMID: 29726782.

14. Levin VA, Bidaut L, Hou P, Kumar AJ, Wefel JS, Bekele BN, et al. Randomized double-blind placebo-controlled trial of bevacizumab therapy for radiation necrosis of the central nervous system. Int J Radiat Oncol Biol Phys. 2011;79(5):1487-95. doi: 10.1016/j.ijrobp.2009.12.061. PubMed PMID: 20399573; PubMed Central PMCID: PMC2908725.

15. Mayo ZS, Halima A, Broughman JR, Smile TD, Tom MC, Murphy ES, et al. Radiation necrosis or tumor progression? A review of the radiographic modalities used in the diagnosis of cerebral radiation necrosis. J Neurooncol. 2023;161(1):23-31. Epub 20230112. doi: 10.1007/s11060-022-04225-y. PubMed PMID: 36633800.

16. Dequesada IM, Quisling RG, Yachnis A, Friedman WA. Can standard magnetic resonance imaging reliably distinguish

recurrent tumor from radiation necrosis after radiosurgery for brain metastases? A radiographic-pathological study. Neurosurgery. 2008;63(5):898-903; discussion 4. doi: 10.1227/01.NEU.0000333263.31870.31. PubMed PMID: 19005380.

17. Kano H, Kondziolka D, Lobato-Polo J, Zorro O, Flickinger JC, Lunsford LD. T1/T2 matching to differentiate tumor growth from radiation effects after stereotactic radiosurgery. Neurosurgery. 2010;66(3):486-91; discussion 91-2. doi: 10.1227/01.NEU.0000360391.35749.A5. PubMed PMID: 20173543.

18. Stockham AL, Tievsky AL, Koyfman SA, Reddy CA, Suh JH, Vogelbaum MA, et al. Conventional MRI does not reliably distinguish radiation necrosis from tumor recurrence after stereotactic radiosurgery. J Neurooncol. 2012;109(1):149-58. Epub 20120526. doi: 10.1007/s11060-012-0881-9. PubMed PMID: 22638727.

19. Mohamedkhan S, Hindocha S, de Boisanger J, Millard T, Welsh L, Rich P, et al. Contrast Clearance Analysis (CCA) to Assess Viable Tumour following Stereotactic Radiosurgery (SRS) to Brain Metastasis in Non-Small Cell Lung Cancer (NSCLC). Cancers (Basel). 2024;16(6). Epub 20240320. doi: 10.3390/cancers16061218. PubMed PMID: 38539550; PubMed Central PMCID: PMC10969132.

20. Kim HY, Cho SJ, Sunwoo L, Baik SH, Bae YJ, Choi BS, et al. Classification of true progression after radiotherapy of brain metastasis on MRI using artificial intelligence: a systematic review and meta-analysis. Neurooncol Adv. 2021;3(1):vdab080. Epub 20210701. doi: 10.1093/noajnl/vdab080. PubMed PMID: 34377988; PubMed Central PMCID: PMC8350153.

21. Kwee RM, Kwee TC. Dynamic susceptibility MR perfusion in diagnosing recurrent brain metastases after radiotherapy: A systematic review and meta-analysis. J Magn Reson Imaging. 2020;51(2):524-34. Epub 20190531. doi: 10.1002/jmri.26812. PubMed PMID: 31150144; PubMed Central PMCID: PMC7004193.

22. Kaufmann TJ, Smits M, Boxerman J, Huang R, Barboriak DP, Weller M, et al. Consensus recommendations for a standardized brain tumor imaging protocol for clinical trials in brain metastases. Neuro Oncol. 2020;22(6):757-72. doi: 10.1093/neuonc/noaa030. PubMed PMID: 32048719; PubMed Central PMCID: PMC7283031.

23. Mathews VP, Caldemeyer KS, Lowe MJ, Greenspan SL, Weber DM, Ulmer JL. Brain: gadolinium-enhanced fast fluid-attenuated inversion-recovery MR imaging. Radiology. 1999;211(1):257-63. doi: 10.1148/radiology.211.1.r99mr25257. PubMed PMID: 10189481.

24. Griffiths PD, Coley SC, Romanowski CA, Hodgson T, Wilkinson ID. Contrast-enhanced fluid-attenuated inversion recovery imaging for leptomeningeal disease in children. AJNR Am J Neuroradiol. 2003;24(4):719-23. PubMed PMID: 12695212; PubMed Central PMCID: PMC8148663.

25. Parmar H, Sitoh YY, Anand P, Chua V, Hui F. Contrast-enhanced flair imaging in the evaluation of infectious leptomeningeal diseases. Eur J Radiol. 2006;58(1):89-95. Epub 20060118. doi: 10.1016/j.ejrad.2005.11.012. PubMed PMID: 16386866.

26. Fukuoka H, Hirai T, Okuda T, Shigematsu Y, Sasao A, Kimura E, et al. Comparison of the added value of contrast-enhanced 3D fluid-attenuated inversion recovery and magnetization-prepared rapid acquisition of gradient echo sequences in relation to conventional postcontrast T1-weighted images for the evaluation of leptomeningeal diseases at 3T. AJNR Am J Neuroradiol. 2010;31(5):868-73. Epub 20091224. doi: 10.3174/ajnr.A1937. PubMed PMID: 20037130; PubMed Central PMCID: PMC7964192.

27. Bossuyt PM, Reitsma JB, Bruns DE, Gatsonis CA, Glasziou PP, Irwig L, et al. STARD 2015: An Updated List of Essential Items for Reporting Diagnostic Accuracy Studies. Radiology. 2015;277(3):826-32. Epub 20151028. doi: 10.1148/radiol.2015151516. PubMed PMID: 26509226.

28. Heyn C, Moody AR, Tseng CL, Wong E, Kang T, Kapadia A, et al. Segmentation of Brain Metastases Using Background Layer Statistics (BLAST). AJNR Am J Neuroradiol. 2023;44(10):1135-43. Epub 20230921. doi: 10.3174/ajnr.A7998. PubMed PMID: 37735088; PubMed Central PMCID: PMC10549939.

29. Mehrabian H, Chan RW, Sahgal A, Chen H, Theriault A, Lam WW, et al. Chemical Exchange Saturation Transfer MRI for Differentiating Radiation Necrosis From Tumor Progression in Brain Metastasis-Application in a Clinical Setting. J Magn Reson Imaging. 2023;57(6):1713-25. Epub 20221011. doi: 10.1002/jmri.28440. PubMed PMID: 36219521.

30. Lin NU, Lee EQ, Aoyama H, Barani IJ, Barboriak DP, Baumert BG, et al. Response assessment criteria for brain metastases: proposal from the RANO group. Lancet Oncol. 2015;16(6):e270-8. Epub 20150527. doi: 10.1016/S1470-2045(15)70057-4. PubMed PMID: 26065612.

31. Peng L, Parekh V, Huang P, Lin DD, Sheikh K, Baker B, et al. Distinguishing True Progression From Radionecrosis After Stereotactic Radiation Therapy for Brain Metastases With Machine Learning and Radiomics. Int J Radiat Oncol Biol Phys. 2018;102(4):1236-43. Epub 20180524. doi: 10.1016/j.ijrobp.2018.05.041. PubMed PMID: 30353872; PubMed Central PMCID: PMC6746307.

32. Shiroishi MS, Castellazzi G, Boxerman JL, D'Amore F, Essig M, Nguyen TB, et al. Principles of T2 *-weighted dynamic susceptibility contrast MRI technique in brain tumor imaging. J Magn Reson Imaging. 2015;41(2):296-313. Epub 20140512. doi: 10.1002/jmri.24648. PubMed PMID: 24817252.

33. Quarles CC, Gochberg DF, Gore JC, Yankeelov TE. A theoretical framework to model DSC-MRI data acquired in the presence of contrast agent extravasation. Phys Med Biol. 2009;54(19):5749-66. Epub 20090904. doi: 10.1088/0031-9155/54/19/006. PubMed PMID: 19729712; PubMed Central PMCID: PMC2767268.

SUPPLEMENTAL FILES

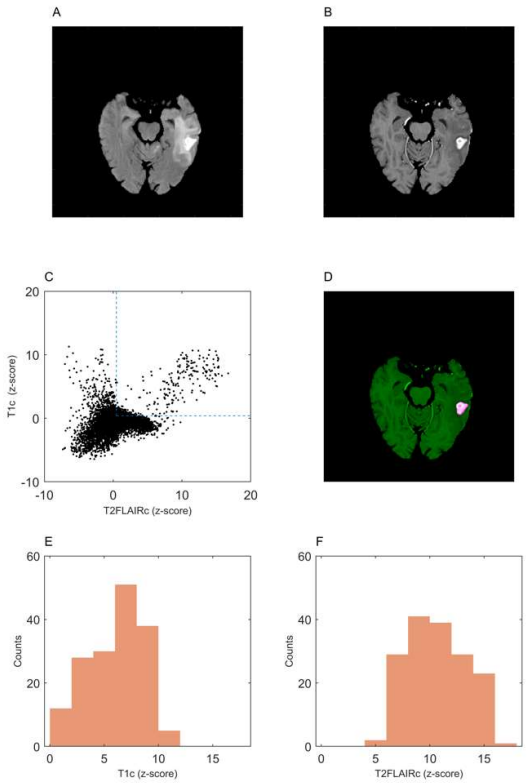


**Supplemental Figure:** Background LAyer STastics segmentation of a treated brain metastasis in the left temporal lobe. The signal intensities for all voxels on contrast enhanced T2 FLAIR (T2FLAIRc) **(A)** and T1 MPRAGE (T1c) **(B)** are plotted in a two-dimensional parameter space **(C)** where each point in the parameter space correlates with signal intensities for a voxel in image space. The signal intensities are normalized relative to the signal intensities of normal brain parenchyma (background layer) cluster derived from a slice of normal brain selected by the user (not shown) and expressed as a z-score. The normalized signal intensity in z-score is calculated as $(S-S_b)/\sigma_b$ where S is the voxel signal intensity, $S_b$ and $\sigma_b$ are the mean and standard deviation of signal intensities for normal grey/white matter respectively. Segmentations are performed by a user applying thresholds (dashed lines) in T1c and T2FLAIRc to select tumor voxels (right upper quadrant). Back-projection of these voxels into image space, grouping of connected voxels and automatic filling of holes produces a segmentation of the whole tumor **(D)**. For the signal intensity analysis in this paper, enhancing tumor voxels were automatically selected by using a threshold of T1c z-score = 0 applied to the whole tumor segmentation. Whole tumor voxels meeting this criteria have signal intensities on T1c which measure above the mean T1c of the background layer and define "enhancement" in this paper. Histograms of enhancing voxels for normalized T1c **(E)** and normalized T2FLAIRc **(F)** for the tumor are shown. For the analysis, all enhancing voxels from the entire 3D tumor volume were aggregated. Segmentations and signal analysis of the entire 3D tumor volume require approximately 1 minute of user time/tumor.